From molecular control to quantum technology with the dynamic Stark effect

Philip J. Bustard,[ab] Guorong Wu,[a] Rune Lausten,[a] Dave Townsend,[c] Ian A. Walmsley,[b] Albert Stolow[a] and Benjamin J. Sussman[*a]

The non-resonant dynamic Stark effect is a powerful and general way of manipulating ultrafast processes in atoms, molecules, and solids with exquisite precision. We discuss the physics behind this effect, and demonstrate its efficacy as a method of control in a variety of systems. These applications range from the control of molecular rotational dynamics to the manipulation of chemical reaction dynamics, and from the suppression of vacuum fluctuation effects in coherent preparation of matter, to the dynamic generation of bandwidth for storage of broadband quantum states of light.

1. Introduction

There are deep connections between the quantum control of chemical processes and the burgeoning development of technologies based on quantum information. Both utilize electromagnetic forces which govern the static and dynamic behaviour of quantum systems containing electrons. The first and most famous example of external field control over quantum states is the Stern-Gerlach experiment where a static but spatially inhomogeneous magnetic field was used to modify the translational states of free silver atoms. More generally, time-dependent electromagnetic interactions may be applied to the manipulation of quantum systems, perhaps ideally using lasers fields.[1,2] The electric field strengths generated by modern short pulse lasers can exceed those which bind electrons to matter. Furthermore, these electric interactions can be rapidly varied, on time scales comparable to those of internal motions within molecules. Ultrafast lasers make an ideal tool for the manipulation of quantum systems using the these electrodynamic interactions. As is discussed in more detail below, we will be particularly interested in the second order (quadratic) non-resonant dynamic Stark effect (NRDSE). The first order (linear) Stark effect directly induces oscillations in the target quantum system at the frequency of light which, particularly for visible light fields, may be too high for certain purposes. The NRDSE, by contrast, exploits the response of a quantum system to the intensity envelope of a laser pulse rather than the oscillating electric field. As the envelope frequencies in a femtosecond laser pulse are on the time scale of molecular vibrations and rotations, the NRDSE is well suited to the control of quantum dynamics in molecules. That the interaction is non-resonant means that it can be described by use of a polarizability and, hence, the only *a priori* requirement of the quantum system is that it have non-zero polarizability. We will also make use of the non-perturbative nature of the matter-field interaction wherein the usual

[a]Steacie Institute for Molecular Sciences, National Research Council of Canada, 100 Sussex Drive, Ottawa, Ontario, K1A 0R6, Canada. E-mail: ben.sussman@nrc.ca
[b]Clarendon Laboratory, University of Oxford, Parks Road, Oxford, OX1 3PU, UK
[c]School of Engineering and Physical Sciences, Heriot-Watt University, Edinburgh, EH14 4AS, UK

spectroscopic picture of transitions will fail. The latter is based on a converging power series expansion in electric field strength, where the complex coefficient of each term is the appropriate order of electric susceptibility. For the NRDSE under consideration here, the non-perturbative interaction extends to all orders but in a specific way, as is discussed in more detail below. Importantly, this means that the quantum transition probabilities in the field cannot be understood by consideration of the linear (or non-linear) Fourier power spectrum of the laser pulse. Rather, the NRDSE interaction can be thought of as the Rabi cycling of stimulated Raman scattering. Using this point of view, we will see that both internal (vibration, rotation, electronic) and external (translation) degrees of freedom may be controlled.

Important to our work is that the NRDSE increases only gradually as the field intensity is increased. Therefore, we can choose non-perturbative intensities at which the quantum system experiences Stark shifts of sufficient magnitude so as to exert an influence over the dynamics, yet produce negligible contributions from other strong field effects such as multi-photon ionization. For non-resonant near-infrared fields, this is in an intensity regime on the order of 10^{12} W cm^{-12}. As a relevant example, this means that we can control the evolution of a chemical reaction on a *given* potential energy surface using strong non-resonant laser fields which do not induce *any* transitions to other potential energy surfaces (*i.e.* other electronic states). In this chemical example, the control is exerted *via* the coordinate dependence of the Stark effect. To make an analogy with skiers going down a hill, the NRDSE interactions modifies the shape of the ski hill (potential energy surface) while the skiers are skiing, but leaves the hill unchanged at the end of the run. Furthermore, the skiers always remain on the same hill throughout.

Closely associated with the field of quantum control is quantum information, computation, and communication (QICC). QICC makes use of the intrinsic uncertainty in quantum mechanics, providing fundamental advantages over operations with classical systems. For these advantages to emerge, however, we will require the accurate articulation and observation of quantum systems. Here too we will see that the NRDSE will play a role. An example discussed in more detail below is a quantum memory which must write a photon to matter and then read the memory to produce an output photon. This procedure is analogous to the well known control protocol STIRAP,[3] which can be used to move population between states in a three-level system. The dynamic bandwidth associated with the NRDSE interaction permits a dramatic speed up of quantum memory devices.

In the following, we will develop the background necessary for understanding the NRDSE interaction and our implementation of it. Various uses of the dynamic Stark effect are then presented and discussed; these diverse applications emphasize the great utility of the dynamic Stark effect in the control and articulation of seemingly disparate quantum systems. We will illustrate its ability to control molecular dynamics such as axis alignment, and chemical dynamics such as branching ratio control in non-adiabatic photodissociation. We then consider the extension of NRDSE control to the non-adiabatic photodissociation of polyatomic molecules where the Stark interaction modifies dynamics at conical intersections.[4] Moving on to quantum technologies, we consider the preparation and amplification of quantum coherence where the NRDSE plays a key role: amplification of Raman coherences. The amplification will utilize strong fields that produce stimulated emission, but also a weak field whose amplitude is designed to control and suppress the effect of vacuum fluctuations. Finally we discuss the role of the dynamic Stark effect in high speed quantum memories and efforts towards the creation of entangled states in solid state materials such as bulk diamond.

2.   Chemical control

The interaction of a control laser field with a molecule can give rise to a quasistatic shift of the energy levels, much like the Stark effect for a system in a static field. The

level shift can be interpreted as being due to an effective potential energy term created by the control laser. For molecules, the effective potential varies with the direction of the principal axis with respect to the field and can be used to align their molecular frame. The potential also varies with nuclear coordinate and electronic state; it can therefore be used to control vibrational motion. When the control laser intensity is increased sufficiently, significant amounts of stimulated Raman emission may be produced. This creates a feedback mechanism in which the Raman emission may also interact to create a potential. Classically, one might not expect this effect because the optical field oscillations are bipolar and therefore may appear to average to zero. However, the interaction energy is generally nonlinear and in this case rectification can occur in the quadratic term. Quantum mechanically the origin of the quadratic potential energy term is the effect of non-resonant states that do not directly participate in the nuclear dynamics, but nevertheless influence the system.

In this section of the paper, we consider the non-resonant dynamic Stark effect (NRDSE)[5,6] and its use as a method of chemical control. In section 2.1 we develop a classical model and an equivalent quantum mechanical model to derive the generalized Raman interaction Hamiltonian for the NRDSE. Some potential applications of this Hamiltonian as a way of controlling rotational motion are then presented in section 2.2. In section 2.3 we consider the use of the NRDSE as a technique for control of vibrational dynamics in molecules.

2.1 Non-resonant dynamic Stark effect

2.1.1 Classical approach.
The classical interaction of a scalar electric field with a static dipole is given by

$$V^{dipole}(t) = -\mu E(t). \tag{1}$$

However, if the charges are not fixed, the applied field can alter or induce the dipole moment, even if there is no static dipole. The dipole can then be written as a Taylor series in the field

$$\mu(E) = \mu_0 + \alpha E + \dots. \tag{2}$$

where μ_0 is a possible static dipole moment and $\alpha = \frac{d}{dE}\mu(E)$. The energy dV required to move a dipole through an electric field variation dE is $dV = -\mu(E)dE$, so that the total induced dipole moment energy is just the sum

$$V(t) = -\int_E \mu(E)dE = -\mu_0 E - \frac{1}{2}\alpha E^2 + \cdots. \tag{3}$$

If we assume the applied laser has a slowly varying envelope $\varepsilon(t)$ the electric field can be written as

$$E(t) = \frac{1}{2}\varepsilon(t)e^{-i\omega t} + c.c. \tag{4}$$

where ε is allowed to be complex to incorporate an optical phase. We can then write out the interaction (3) explicitly using the oscillating field and envelope quantities:

$$V = -\mu_0 E - \frac{1}{8}\alpha\left(\varepsilon(t)e^{-i\omega t} + \varepsilon^*(t)e^{-i\omega t}\right)^2 + \cdots. \tag{5}$$

Although the field here is completely classical, the quantum processes of photon absorption and emission can still be pictured. The terms oscillating as $e^{-i\omega t}$ correspond to absorption (depicted as an upward arrow ↑) and the terms oscillating as

$e^{i\omega t}$ correspond to emission ($\downarrow$).[7] When the product is expanded, three quadratic terms are formed.

$$V = -\mu_0 E - \frac{1}{8}\alpha\left(2|\varepsilon(t)|^2 + \varepsilon^2(t)e^{-i2\omega t} + \varepsilon^{*2}(t)e^{i2\omega t}\right) + \cdots. \tag{6}$$

A two-photon process is then the product of two single photon processes: two-photon absorption ($\uparrow\uparrow$) arises from the term oscillating at $-2\omega t$ and the reverse two-photon emission ($\downarrow\downarrow$) arises from the term oscillating at $2\omega t$. Raman type excitations ($\uparrow\downarrow$, $\downarrow\uparrow$) arise from the two quasi-static cross-terms (hence the factor of $2|\varepsilon(t)|^2$), which are a product of two terms oscillating at ωt and $-\omega t$. The Raman excitations are quasi-static in the sense that the only time dependence they exhibit is due to the envelope.

While the light electrons can respond to the fast optical oscillations, nuclei are too heavy and cannot. Therefore the fast oscillation terms at $\pm 2\omega t$ can be neglected and only the portion responding to the pulse envelope remains. This is equivalent to saying that two-photon absorption or emission are very weak processes when far from resonance with an electronic transition. The remaining slowly evolving portion represents the Stark induced potential

$$V \approx -\mu_0 E(t) - \frac{1}{4}\alpha|\varepsilon(t)|^2. \tag{7}$$

In the presence of a three dimensional field $\mathbf{E}(t) = \frac{1}{2}\boldsymbol{\varepsilon}(t)e^{-i\omega t} + c.c.$ the above formalism yields an interaction given by:

$$V \approx -\boldsymbol{\mu}_0 \cdot \boldsymbol{E}(t) - \frac{1}{4}\boldsymbol{\varepsilon}^*(t)\cdot\boldsymbol{\alpha}\cdot\boldsymbol{\varepsilon}(t). \tag{8}$$

In summary, the classical approach indicates that, in the presence of an oscillating electric field, a dipole moment may be induced that interacts with the field to produce a quadratic potential. The original dipole interaction remains, but it is augmented by a term quadratic in the field strength. Importantly, it should be noted that while the interaction is quadratic, the interaction appears directly in the Hamiltonian: in terms of quantum mechanical perturbation theory, the influence will be to all orders 2,4,6,…. There are two limits for this general interaction potential: dipole dominated or Raman dominated. Which term dominates depends on the optical frequency and the system matrix elements and energy levels. For purposes of rotational and vibrational control, the optical fields are usually chosen to be non-resonant such that the Raman term dominates.

2.1.2 Quantum approach.
In the transition to semi-classical quantum mechanics, the classical induced Hamiltonians (7) or (8) could be inserted directly into Schrödinger's equation. However, this is not formally correct since it replaces the operator μ with its expectation value. Only the true dipole interaction $V(t) = -\mu E(t)$ should be used and a fully quantum approximation should be investigated. There is no reason to expect identical results from the two approaches although it turns out that the quantum approach gives approximately the same answer, under a more stringent set of limits.

Consider a non-degenerate two-level system starting with a fully populated ground state a and empty excited state b which are coupled by an oscillating field.

$$i\dot{a} = \omega_a a - \mu_{ab}E(t)b \tag{9}$$

$$i\dot{a} = \omega_b b - \mu_{ba}E(t)a \tag{10}$$

The equation for b can be formally integrated† and inserted into the equation for a. In this case, the equation for a is:

$$i\dot{a} = \omega_a a - i\mu_{ab}E(t)e - i\omega_b t \int_0^t \mu_{ba} a E(t')e^{i\omega_b t'}dt' \tag{11}$$

Any dependence on b has been eliminated, but a new term replaces its effect on state-a. The most obvious point is that the new term is quadratic in $E(t)$, like the quadratic Stark effect. However, the amplitude a appears within the integral, suggesting that this is not yet a simple potential energy term.

To demonstrate that this is a potential term, the next step is to approximate the integral and see if the classical approach can be recreated. The integral is rewritten to have the product of a slow part which cannot be analytically integrated and fast oscillating part which can:

$$\int_0^t \left(e^{i\omega_b t} (\tfrac{1}{2}\mu_{ba}\varepsilon(t)e^{-i\omega t} + c.c.)e^{-i\omega_a t} \right) \left((e^{i\omega_a t}a)dt \right) \tag{12}$$

Since a is time dependent it will have some spectral content. The spectral content will consist of a portion at its eigenvalue ω_a and another portion at other frequencies induced by the applied field and resulting dynamics. If the spectral content at ω_a dominates, $e^{i\omega_a t}a$ will be slowly varying (i.e., its time derivative is appropriately small), then the integral can be integrated by parts and the surface term dropped due to small time variations:

$$\frac{1}{2i}\frac{\mu_{ba}\varepsilon(t)}{\omega_b - \omega_a - \omega}e^{i(\omega_b - \omega)t}a + \frac{1}{2i}\frac{\mu_{ab}\varepsilon^*(t)}{\omega_b - \omega_a + \omega}e^{i(\omega_b + \omega)t}a \tag{13}$$

When the laser frequency ω is near resonance with the level spacing $\omega_b - \omega_a$, the second term dominates and the first term may be neglected. Here, both terms are kept so that the off-resonance case is included. The integral is now inserted back into (14) and the rotating wave approximation is taken to eliminate all fast oscillating terms:

$$i\dot{a} = \omega_a a - \frac{1}{4}\left(\frac{\mu_{ab}\varepsilon(t)\mu_{ba}\varepsilon^*(t)}{\omega_b - \omega_a - \omega} + \frac{\mu_{ba}\varepsilon^*(t)\mu_{ab}\varepsilon(t)}{\omega_b - \omega_a + \omega} \right)a \tag{14}$$

or

$$\dot{a} = \omega_a a - \frac{1}{4}\varepsilon^*(t)\alpha\varepsilon(t)a \tag{15}$$

where the dynamic polarizability is

$$\alpha(\omega) = \left(\frac{\mu_{ab}\mu_{ba}}{\omega_b - \omega_a - \omega} + \frac{\mu_{ba}\mu_{ab}}{\omega_b - \omega_a + \omega} \right). \tag{16}$$

This form recreates the classical induced potential (7) when there are two states.

To extend beyond the two-state approximation is relatively straightforward. When interested in the dynamics in state a and multiple other non-resonant states are included, the calculation is essentially the same (although, strictly speaking, the approximations are stronger[5]). In this case, the polarizability in a state a depends on the sum over all non-resonant states b:

---

† The most convenient form is achieved by transforming to the interaction picture, eliminating b, and then transforming back.

$$\alpha_a^{ij}(\omega) = \sum_b \left(\frac{\mu_{ab}^i \mu_{ba}^j}{\omega_b - \omega_a - \omega} + \frac{\mu_{ba}^i \mu_{ab}^j}{\omega_b - \omega_a + \omega} \right) \qquad (17)$$

where the Cartesian indices i,j have been included for the vector case. The Schrödinger equation is now written as:

$$i\dot{a} = Ha - \frac{1}{4}\boldsymbol{\varepsilon}^*(t) \cdot \boldsymbol{\alpha} \cdot \boldsymbol{\varepsilon}(t)a \qquad (18)$$

and the induced potential, as in the classical case

$$V_{NRDSE} = -\frac{1}{4}\boldsymbol{\varepsilon}^*(t) \cdot \boldsymbol{\alpha} \cdot \boldsymbol{\varepsilon}(t) \qquad (19)$$

is recovered. For the case of multiple spectrally distinct fields centered at frequencies ω_p, the field may be written

$$\mathbf{E}(t) = \frac{1}{2}\sum_p [\boldsymbol{\varepsilon}_p(t)e^{-i\omega_p t} + c.c.] \qquad (20)$$

so the potential generalizes to,

$$V_{NRDSE} = -\frac{1}{4}\sum_{p'p} \boldsymbol{\varepsilon}_{p'}^*(t) \cdot \boldsymbol{\alpha} \cdot \boldsymbol{\varepsilon}_p(t)e^{-i(\omega_p - \omega_{p'})t}. \qquad (21)$$

This Hamiltonian is responsible for all of the dynamics induced by the NRDSE, including the well-known molecular frame alignment.

2.2 Alignment with the NRDSE: adiabatic and non-adiabatic techniques

As with the evolution of many other quantum systems, NRDSE control interactions may be separated into one of two categories: those which are *adiabatic*, and those which are *non-adiabatic*. For the control dynamics to be adiabatic, the interaction Hamiltonian must only undergo a small fractional change in a typical period of the unperturbed system. A system starting in an eigenstate of the initial Hamiltonian will then always remain in the corresponding eigenstate of the perturbed Hamiltonian. To violate the condition for adiabatic evolution, the perturbation amplitude or time variation may be increased, leading to transitions between the perturbed states. An examination of (21) reveals that the degree of adiabaticity in a NRDSE control experiment is determined by the applied field strength and its temporal profile, as compared to the timescale of the nuclear rotational, or vibrational motion. Vastly different control outcomes can be achieved in molecules by varying these two parameters. In this section we discuss adiabatic and non-adiabatic control by the NRDSE for the specific case of molecular alignment;[8–11] molecules are said to be aligned when an applied field defines order with respect to a space-fixed axis. This discussion involves a more detailed consideration of Raman scattering, and so we briefly introduce this phenomenon before proceeding.

2.2.1 Raman scattering.
In a Raman process, an input pump field scatters off a molecule and a new field is produced at a longer Stokes wavelength (fig. 1). One photon of the pump is destroyed and a longer wavelength photon at the Stokes frequency is created. Energy is conserved and so the deficit is deposited in the system as a rotational excitation at the pump-Stokes energy differences ω_{pS}, depicted in fig. 1 as between states 0 and 2. This figure shows the specific case of spontaneous Raman scattering, where only a pump field is incident on the medium and emission to the Stokes field is stimulated by the vacuum fluctuations. A theoretical description of spontaneous Raman scattering requires quantization of the Stokes field, which is
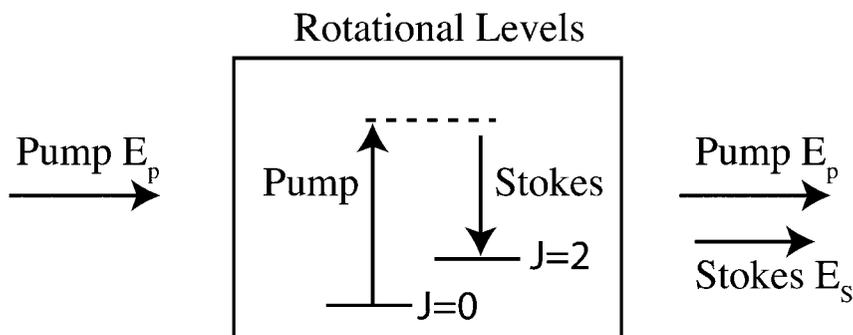
Rotational Levels

Fig. 1 A spontaneous rotational Raman scattering process. An input field excites the medium and a Stokes field is generated to conserve energy and momentum. In the photon perspective a pump photon is destroyed and a Stokes photon and rotational excitation quantum are created. The energy difference between pump and Stokes is the energy difference between states $J = 2$ and $J = 0$. If the pump is short, it may have sufficient bandwidth so that spectrum is present at the Stokes wavelength, thus stimulating the emission of Stokes light.

beyond the scope of the semi-classical model discussed herein. We note, however, that in the absence of an input Stokes field, the phase of the output Stokes field is random due to its quantum mechanical origin.[12,13] Stimulated Raman scattering occurs when the Stokes field, and the Raman excitation, are made to grow nonlinearly by increasing the Raman gain of the medium such that the Stokes field can stimulate the emission of further Stokes photons. For transient phenomena, where the Raman excited molecules maintain a well-defined phase relationship with the Stokes field, the Raman gain is enhanced by increasing the number of scattering molecules, or by increasing the fluence of the pump field.[13]

Should the population in the upper energy level become large enough, the process can be reversed, with the Stokes field producing anti-Stokes light at the shorter pump wavelength. Because the cross sections are so small, the generation of Raman scattered light is often ignored in alignment experiments, however its mechanism is intimately related to non-adiabatic alignment approaches.

In order to discuss potential mechanisms of alignment by the NRDSE, it is helpful to explicitly write the control field as an interaction of two spectrally distinct input fields $E = E_p + E_S$, the pump p and the scattered Stokes S fields, both assumed to be slowly varying. Eqn (21) then has the following form:

$$V_{NRDSE} = V_p + V_S + V_{pS} + V_{Sp}. \tag{22}$$

where

$$V_p = -\frac{1}{4}\varepsilon_p^* \cdot \boldsymbol{\alpha} \cdot \varepsilon_p \quad \text{standard alignment} \quad c.f., \ (8, 19) \tag{23}$$

$$V_S = -\frac{1}{4}\varepsilon_S^* \cdot \boldsymbol{\alpha} \cdot \varepsilon_S \quad \text{Stokes alignment} \tag{24}$$

$$V_{pS} = -\frac{1}{4}\varepsilon_p^* \cdot \boldsymbol{\alpha} \cdot \varepsilon_S e^{-i\omega_{pS}t} \quad \text{Stokes scattering} \tag{25}$$

$$V_{Sp} = -\frac{1}{4}\varepsilon_S^* \cdot \boldsymbol{\alpha} \cdot \varepsilon_p e^{i\omega_{pS}t} \quad \text{anti} - \text{Stokes scattering}. \tag{26}$$

The four terms each result in different modification of the molecular motion. The first term V_p contains no rapid time-dependence since the field is assumed to be slowly varying. As a result, the frequency spectrum of the V_p term is not resonant with any non-degenerate rotational levels and the V_p term is therefore responsible for adiabatic alignment; this is discussed further in section 2.2.2. Similarly, the second term V_S represents the alignment potential due to the Stokes field, which we also assume to be slowly-varying. In the absence of a large input Stokes field, or stimulated emission due to large Raman gain, V_S is usually small compared to V_p and can be neglected. Importantly, the inclusion of the pump and Stokes fields has resulted in the appearance of an oscillation at the beat frequency at ω_{pS} in the V_{pS} (Stokes) and V_{Sp} (anti-Stokes) scattering terms. This beat frequency may efficiently drive the internuclear dynamics when ω_{pS} is tuned close to resonance with a rotational energy level splitting. Physically, this is because the electrons respond to the fast oscillations of the field but the heavier nuclei cannot. The electrostatic coupling of the electrons to the nuclei means that modulating the control field intensity at ω_{pS} will parametrically drive the nuclear motion at this frequency, thereby transferring population between the rotational levels by Stokes scattering. The V_{Sp} term can similarly drive transitions in the opposite direction by anti-Stokes scattering.

2.2.2 Adiabatic and non-adiabatic alignment. The critical molecular timescale in determining the adiabaticity of alignment is the timescale of rotational motion $\tau_{rot.}$ For an applied field to adiabatically induce alignment, the control pulse intensity must vary slowly in time, compared with τ_{rot}. This is typically achieved by using a smoothly-varying control pulse of duration τ satisfying[8] $\tau \gg \tau_{rot}$. As the field is applied it 'dresses' the system and, taking advantage of the adiabatic theorem, slowly transports an unaligned state to an aligned state. If the field is slowly turned back off, the aligned state will adiabatically evolve to its original unaligned state, up to a global phase shift. In this adiabatic limit, only the V_p term is significant, and emission to the Stokes field can be neglected.

The essential feature of an adiabatic aligning potential V_p is that it contains no oscillating exponential component. It is basically a DC field that follows the pump pulse envelope; *i.e.* the frequency spectrum of V_p is not resonant with different states. Since it is not resonant, following the interaction the state populations remain unchanged. This is the mechanism of adiabatic alignment. To observe this explicitly, Fermi's Golden rule can be used to determine whether or not a transition occurs. From the time-domain version of Fermi's Golden rule, the amplitude for state $J = 2$ following excitation from state $J = 0$ can be written in first order perturbation theory for V_P as

$$c_2(t) \approx \frac{i}{4} \int_{-\infty}^{t} e^{-i\omega_{02}t} \langle 2|, \boldsymbol{\varepsilon}_p^* \cdot \boldsymbol{\alpha} \cdot \boldsymbol{\varepsilon}_p |0\rangle dt. \tag{27}$$

This is a finite time Fourier transform, with a slow varying argument $\langle 2|, \boldsymbol{\varepsilon}_p^* \cdot \boldsymbol{\alpha} \cdot \boldsymbol{\varepsilon}_p | 0\rangle$. At late times there is no population excitation since $c_2(\infty) = 0$. At early times, while the pump $\boldsymbol{\varepsilon}_p$ is on, amplitude c_2 is excited (the molecule is aligned) due to apparent bandwidth introduced by truncating the integral at time t, instead of at infinity. That is, the finite time integral is physically equivalent to the case of a pump $\boldsymbol{\varepsilon}_p$ that is suddenly switched off at time t. A sudden turn off generates large resonant bandwidth. This leads to the notion of 'switched wave-packets', discussed below. At later times, when the pulse is over, the Fourier transform samples the full-time excitation and finds no resonant excitation which would leave population in the excited state: at first the system experiences a large resonant bandwidth, and does not discover that the excitation is really non-resonant until the pulse is over. This demonstrates that an adiabatic pulse aligns a molecule even if there is no resonant

This journal is © The Royal Society of Chemistry 2011

excitation, because while the pulse is applied the molecule experiences greater apparent bandwidth then is actually present, and population is excited, thus generating adiabatic alignment. The adiabatic alignment effect may also be understood by diagonalizing the full Hamiltonian to introduce pendular states which are hybrids of the field-free rotational eigenstates.[9]

Alignment *via* non-adiabatic means can be achieved by increasing the rate of change of the interaction Hamiltonian V_{NRDSE} with respect to the frequency-splittings of the molecule rotational levels. In this case, the frequency spectrum of the interaction Hamiltonian will come into resonance with the rotational level splittings such that population can be transferred from one rotational level to another. A simple way to achieve this[14] is to apply a Stokes field in addition to the pump field such that $\omega_{pS} \approx (\omega_{J+2} - \omega_J)$ where ω_J is the frequency of the rotational level with quantum number J. If the lower energy level is populated more than the upper level, the V_{pS} term will resonantly transfer population from the lower level to the upper level; if the population inversion is reversed, the V_{Sp} term will dominate and transfer population in the opposite direction. The phase of the coherent rotational motion induced by this process is set by the phase difference of the pump and Stokes fields. In the absence of decoherence mechanisms such as collisional dephasing, non-adiabatic excitation of the coherent rotational motion may result in field-free superpositions of the initial rotational eigenstates after the control field is turned off. The generation of field-free molecular alignment is key theme in emerging methods for the study of ultrafast molecular dynamics.[8]

Instead of applying an external Stokes field, in some instances significant alignment may be generated by simply increasing either the fluence of a slowly-varying pump, or the number of scattering molecules, so that spontaneous emission to the Stokes field can reach the regime of stimulated Raman scattering. As the pump field propagates, positive feedback from the Stokes field stimulates further Stokes emission. In this way, energy is transferred from the pump field to the medium as the pump and Stokes drive transitions among the rotational levels. A key point to note, however, is that the phase of such a Raman excitation will be random on any given laser shot due to the quantum mechanical origin of the Stokes light. It is therefore not possible to probe any ultrafast rotational dynamics using short probe pulses as there is no phase relationship between the molecules and the probe. Quantum coherence amplification is discussed in section 2.4 as a solution to this problem.

An extreme example of non-adiabatic alignment is *impulsive* alignment, where a short pulse with duration at or below the timescale of typical rotational motion $\tau \leq \tau_{rot}$ is used to induce alignment by impulsive stimulated Raman scattering.[15] The bandwidth of a pulse $\Delta\omega$ is inversely related to its duration as $\Delta\omega \sim 1/\tau$. Therefore, impulsive pulses have sufficient bandwidth to overlap with an initial state and a target state. As the short pulse consists of a broad coherent phase-locked spectrum, the subsequent phases of the target molecules' states are locked by the impulsive excitation and are therefore left in a superposition. The energy deposited in the molecules by the Raman scattering interaction results in a red-shifting of the pulse spectrum. The broad bandwidth of short pulses makes a clear separation of V_{NRDSE} into distinct frequency components difficult. Typically this is dealt with theoretically by considering only the V_P term in V_{NRDSE} while relaxing the condition that the pulse envelope be slowly-varying.

2.2.3 Alignment potentials. The type of order induced by an alignment potential depends principally on the molecular structure, the control field polarization, and the control field temporal profile. In systems where sufficient numbers of molecules are excited, feedback from the molecules can significantly alter the control field. Propagation then becomes a significant factor, resulting in spatial variation of the interaction Hamiltonian V_{NRDSE} and of the aligned sample. For example, in the case where a pump field and a Stokes field are applied in two-photon

resonance with a rotational transition, the Stokes field grows at the expense of the pump field as it propagates through the medium, resulting in growth of the rotational coherence along the direction of propagation. In this section, we consider the effect of the control field polarization and the control field temporal profile on the alignment. We then use experimental results to highlight the effect of the control field temporal profile, and contrast adiabatic with non-adiabatic alignment.

From the general form of the non-resonant Stark potential (8) or (19), the angular dependence of the aligning force can be demonstrated. We use the coordinate system shown in Fig. 2 for the ensuing discussion. For molecules symmetric about the major axis, the polarizabilities on the two minor axis are equal such that $\alpha_1 = \alpha_2$. When an electric field vector is polarized along the z direction such that

$$\boldsymbol{\varepsilon} = \varepsilon_0(t) \begin{bmatrix} 0 \\ 0 \\ 1 \end{bmatrix} \tag{28}$$

the interaction (21) then simplifies to

$$V(t) = -\frac{1}{4}|\varepsilon_0(t)|^2 \left(\alpha_1 + (\alpha_3 - \alpha_1)\cos^2(\theta) \right). \tag{29}$$

Therefore the molecules experience a Stark shift which is equivalent to adding or *shaping* a potential energy surface so as to create a minimum that varies as $\cos^2(\theta)$. The potential well minimum draws the principal axis of the molecule toward the z coordinate axis and aligns the system. Note that since the interaction pulls toward both $\theta = 0, \pi$ the molecules do not orient themselves with respect to one end or the other; for orientation this interaction cannot be used alone.

For consideration of circular polarized fields, the equations can be simplified by choosing a different orientation for the aligning field. The equations are simplified for circular polarization in the xy-plane:
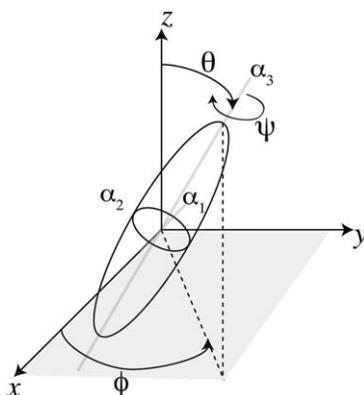

Fig. 2 A molecule (black ellipsoid) and its principle axes. The Euler angles θ and ϕ relate the principle axis of the molecule to the space-fixed frame. The principal axes of the polarizabilities are shown in grey, aligned here with the (moment of inertia) principle axes of the molecule. The Euler angle ψ is a rotation about the main principal axis. The polarizabilities α_i are shown along the grey axes. For example, application of a linear laser field polarized along z creates an aligning potential that aligns the principal axis toward the z axis.

$$\boldsymbol{\varepsilon} = \frac{\varepsilon_0(t)}{\sqrt{2}} \begin{bmatrix} i \\ 1 \\ 0 \end{bmatrix} \qquad (30)$$

The interaction then simplifies to

$$V(t) = -\frac{1}{4}|\varepsilon_0(t)|^2 \left(\alpha_3 + \frac{1}{2}(\alpha_3 - \alpha_1)\sin^2(\theta) \right). \qquad (31)$$

In contrast to the linear polarized case, now the potential energy is minimized when $\theta = \pi/2$. The effect of circularly polarized light is thus to pull the molecule to the xy-plane in which the light field rotates.

2.2.4 Field-free molecular alignment.

The application of nonresonant fields can be used to align molecules in induced potentials. However, while the aligning potentials are on, the molecular states are subject to level shifts. This field-induced restructuring will significantly hinder the interpretation of any spectroscopic or dynamics studies in terms of field-free behaviour, the general goal. For dynamical studies, molecular alignment methods should be field-free. In this section, we discuss two alternative methods for the preparation of field-free molecular alignment using linearly-polarized pump fields: switched wave-packets,[16,17] and impulsive stimulated Raman scattering.[10] To induce field-free alignment, each of these techniques are necessarily non-adiabatic. The relevant potential for these alignment fields is (29). The degree of molecular alignment was measured by detecting the transient birefringence of the sample as a function of time using a pump–probe technique. In the absence of an aligning potential, the molecules are randomly aligned and so no birefringence is detected. By contrast, alignment of the sample along an axis induces a directional dependence in the polarizability, and therefore net birefringence. The probe pulse was linearly-polarized at 45° to the aligning field polarization; measurement of the polarization-rotated component through a high-extinction ratio polarizer as part of a Kerr cell is then a sensitive way to sample the birefringence, and thus alignment, of the sample.[11]

In the switched wave-packet (SWP) technique, a 100 ps, 1.064 μm pump pulse is truncated using a plasma shutter to provide a control pulse with a slowly increasing intensity to its peak, followed by a sudden drop of intensity to zero in a few tens of femtoseconds. Fig. 3 (top) shows the resulting polarization-rotated component of an 80 fs, 800 nm probe pulse detected using a photo-multiplier tube (PMT) after propagation through a sample of CO_2 molecules at 300 Torr. It should be noted that when the pump and probe pulses overlap in time, the measured birefringence includes a component due to the extremely transient (field-following) electronic response and the slower nuclear alignment response; only the latter is present at positive probe delays however. At negative probe delays, the birefringence smoothly increases as the sample is adiabatically driven to align with the pump polarization by the slowly increasing intensity. The birefringence signal drops sharply at zero-delay as the pump pulse is truncated, however periodic revivals are seen in the birefringence signal at larger delays. Coherence is left among the rotational levels because the pump pulse is turned off much more rapidly than the time-scale of rotational motion in CO_2, thus projecting the field-perturbed state on to the field-free eigenstates. The periodic revivals occur due to rephasings of the rotational wavepacket as it freely evolves in the absence of the control field. The revivals correspond to times at which the molecules are aligned but no external field is present. These revivals are very useful for the dynamical study of molecular frame properties.

In the second experiment, a 55 fs, 800 nm pump pulse was used to induce alignment in N_2 by impulsive stimulated Raman scattering. The time-dependent
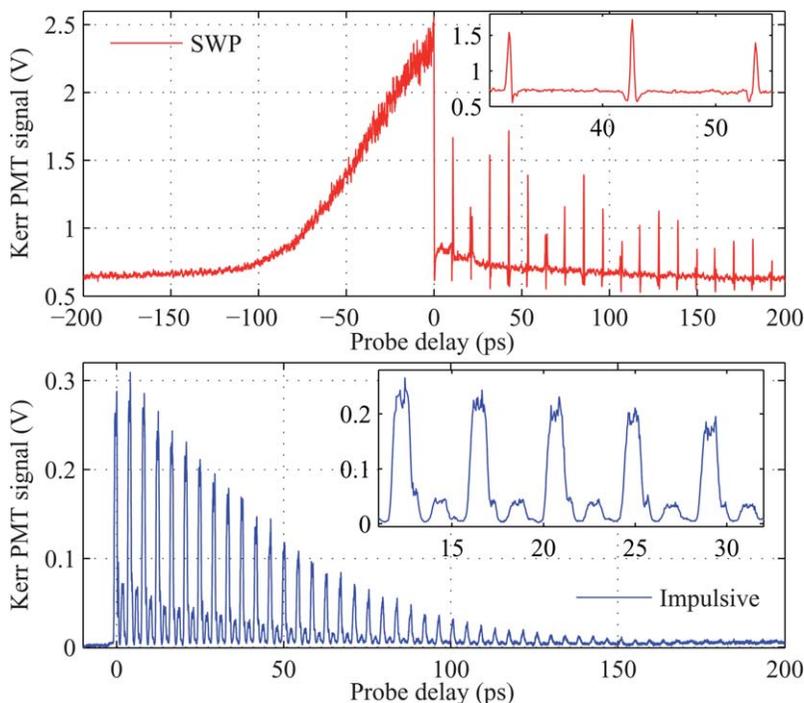
Fig. 3 Kerr cell detection of field free alignment for two contrasting control fields. Top: A switched wave-packet (SWP) technique is used to adiabatically align CO_2 molecules with the smoothly increasing linearly-polarized pump pulse envelope. The pump pulse is rapidly turned off, projecting the molecules onto a superposition of the field-free rotational eigenstates. Revivals in the molecular alignment are seen at positive probe delay times due to periodic rephasings of the non-adiabatically prepared rotational wave-packet. The inset shows the structure of the revival signal in detail. Bottom: A sample of N_2 molecules is impulsively aligned by a linearly polarized 55 fs pump pulse. Revivals in the alignment signal are again apparent due to the periodic rephasing of the non-adiabatically prepared rotational wave-packet.

birefringence signal is plotted in Fig. 3 (bottom). At negative probe delay times, no birefringence is detected using the 400 nm probe pulse, however prompt birefringence is induced within tens of femtoseconds of zero-delay. As with the SWP experiment, due to the non-adiabatic nature of the control field potential, coherence is left among the rotational levels. The resulting rotational wave-packet periodically rephases resulting in revivals in the birefringence signal. In both experiments, the birefringence signal decays as a function of time due to collisional dephasing of the rotational coherence, and intrinsic dephasing of the wave-packet caused by centrifugal distortions to the simple rotor Hamiltonian.[18]

2.3 Vibrational control

Many chemical reactions can be thought of as trajectories on vibrational potential energy surfaces which start as reagents, proceed over a barrier, and end as products. Catalysts often enhance reactions by exerting multi-polar electric forces that reduce the barrier. In a similar manner, the non-resonant dynamic Stark effect (NRDSE) can be used to modify the barriers of a chemical reaction on ultrafast timescales in order to control the outcome of a reaction.

Vibrational control using the NRDSE has been applied to an important class of photochemical reactions: nonadiabatic processes. These processes, such as internal

conversion or intersystem crossing, entail charge rearrangements that occur along a reaction path at the intersections of potential energy surfaces and act as triggers of the ensuing chemistry. Chemical branching ratios in nonadiabatic processes are very sensitive to the intersection geometry, and therefore the dynamic modification of these processes is an important application of the NRDSE. So far, control on chemical branching ratios using the NRDSE has only been demonstrated on a diatomic molecule. The specific example was the nonadiabatic photodisociation of IBr.[19]

In IBr, there is an avoided crossing between 2(B) and 3(Y) excited states, which leads to two chemically distinct, neutral atomic channels: IBr → I + Br($^2P_{3/2}$) and I + Br*($^2P_{1/2}$).[20] An infrared NRDSE field can be used to modify the curve-crossing barrier at a specific time, thus promoting the yield of one chosen product over another. In the experiment, the reaction was initiated by a 100 fs laser pulse centered at 520 nm, above the dissociation limit for both channels. A strong, time-delayed non-resonant 1.7 μm infrared pulse, 150 fs in duration, was used as the control field. About 60 ps after the pump and control pulses, a third weak pulse at 304.5 nm was used to spectroscopically detect free, neutral ground state iodine atom products via (2 + 1) resonance-enhanced multiphoton ionization (REMPI). Measurement of the iodine atom kinetic energy distribution permits unambiguous determination of the Br*/Br product branching ratio, via conservation of kinetic energy and linear momentum. A dramatic variation of the overall integrated Br*/Br branching ratio as a function of control pulse delay was observed. At early and late times, the branching ratio was identical to that of the molecule under field-free conditions. Although the product branching ratios were controlled by the NRDSE field, the asymptotic recoil velocities of I atom fragments remained unmodified—they always matched those of the field-free dissociation. These results demonstrate that there is no significant net absorption of photons during the NRDSE interaction: there are no real electronic or ionizing transitions due to the application of the control pulse. There are two time delays when the reaction outcome is critically sensitive to the control field: (i) during initiation, and (ii) during traversal of the crossing point. If the NRDSE pulse is applied simultaneously with the initiation pulse, the reaction begins on a Stark-shifted potential energy surface. The Stark lowering of the ground state has an effect equivalent to spectrally red-shifting the pump laser wavelength. The result is that, after the control pulse turns off, the wave-packet velocity is reduced at the crossing point, decreasing the 'hopping' probability and enhancing the Br channel. An enhancement of 60 percent of Br yield at the expense of the Br* channel was observed. Application of the control pulse during traversal of the crossing point shifts and lowers the adiabatic barrier, thereby increasing the diabatic Landau–Zener hopping probability[21] and thus production of Br*. The enhancement of the Br* channel was more than 30 percent. The fractional change of peak-to-valley contrast of the branching ratio was over 90 percent and, importantly, due to the non-perturbative nature of the interaction, control was exerted on 100 percent of the reacting population.

An extension of the NRDSE control scheme to non-adiabatic dynamics at conical intersections in polyatomic molecules is a longstanding goal. However, the intrinsic multidimensionality of polyatomic systems makes this extension challenging. In diatomic molecules, the branching of chemical processes at an avoided crossing is determined by the velocity of wave-packet, the relative slopes of the two coupled potential energy curves, and their coupling strengths. In polyatomic molecules, the potential energy surfaces are multidimensional hypersurfaces, and the zero dimensional avoided crossing of diatomic molecules becomes a N^{int}-2dimensional seam of conical intersection (CI), where N^{int} is the number of internal degrees of freedom.[22] The branching between adiabatic and diabatic dynamics at the CI is largely determined by the local topography. However, there is evidence that the speed and direction of approach of the wave-packet to the CI may also affect the diabatic versus adiabatic branching.[23] Wave-packets on excited state potential

energy surfaces may also decay through more than one type of CI. The routing of the wave-packet to different CIs is certainly dependent on details of the potential. Therefore, modification of potentials due to the NRDSE would be expected to change this routing and, hence, control the relative contributions of the electronic channels involved in the dynamics. In addition, modification of potentials using the NRDSE may also lead to different state distribution amongst the products within each channel, a phenomenon which is absent in diatomic cases. NRDSE control of chemical processes in polyatomic molecules is expected to be much more challenging and requiring of more detailed information on dynamical pathways. In return, the studies of NRDSE control over polyatomic molecule electronic branching ratios may also provide new insights into the dynamics of these systems. These developments will require considerable experimental and theoretical effort.

In order to extend the control of diatomics to a polyatomic system exhibiting electronic branching control *via* the NRDSE, we must begin by experimentally characterizing the field-free dynamics. As a candidate system, we have chosen to investigate the UV photodissociation of N-methylpyrrole (NMP), which has a number of appealing features. Experiments demonstrated the existence of methyl radical elimination channels with differing kinetic energy release (termed here 'fast' and 'slow').[24,25] The relative contribution of these channels varies with excitation energy. A sudden change in the slow *versus* fast methyl radical branching ratios occurs around 239 nm excitation. At wavelengths longer than 239 nm, there are two clear maxima in the CH_3 radical kinetic energy distribution, corresponding to slow and fast products. When the pump wavelength is tuned to 238 nm or below, the fast CH_3 radical channel apparently disappears. At these wavelengths, the molecule is vibronically excited to the $S_1(^1A_2,\pi\sigma^*)$ state. At even shorter wavelengths, the initial excitation is to the dipole allowed $\pi\pi^*$ state, which has a maximum around 217 nm.[26] However, the kinetic energy distribution of CH_3 has a very similar profile to the one at 238 nm. It was suggested that the slow *versus* fast CH_3 branching is due to the diabatic *versus* adiabatic splitting of the excited state wave-packet upon traversal of the CI connecting the first excited state (S_1) with the ground state (S_0), as shown in Fig. 4. One wave-packet component decays along the repulsive $\pi\sigma^*$ surface (which is the S_1 state in the Franck–Condon (FC) region and has 3s
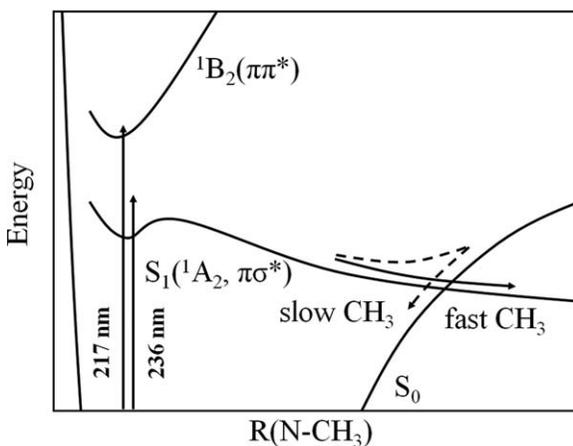

Fig. 4 Schematic potential energy curves for the ground state and two singlet excited states of NMP plotted as a function of $R(N\text{-}CH_3)$.[48] This figure also illustrates the branching of photodissociation at the S_0/S_1 conical intersection. The direct dissociation along the repulsive $\pi\sigma^*$ surface leads to fast CH_3 radicals, while the dissociation of the hot ground state following internal conversion from the S_1 state leads to slow CH_3 radicals. The vertical arrows indicate the pump wavelengths.

Rydberg character), generating the fast CH_3 radical elimination. The other wave-packet component decays to the ground state *via* internal conversion: the hot ground state molecule subsequently undergoes statistical unimolecular dissociation to yield the slow CH_3 radical channel. In order that control be effective, the time scale of the dynamics must be accessible with available ultrafast control lasers. For these reasons, the photodissociation results and theoretical calculations[27,28] on the relevant potential energy surfaces make NMP a promising candidate for NRDSE control. However, the nonadiabatic excited state dynamics of NMP, especially the nature of the dependence of the slow *versus* fast branching ratio upon excitation energy are not well understood and require further study. Time-resolved measurements allow us to directly follow the wave-packet evolution on the excited state potential energy surfaces, and will provide complementary information. Due to the lack of previous experimental research, we performed femtosecond time-resolved photoelectron spectroscopy (TRPES)[29] studies. This is very important in understanding the dynamics of the branching and its excitation energy dependence, which is critical to the implementation of coherent control of NMP photodissociation. Measurements were made at three different pump laser wavelengths: (i) 242 nm, where both slow and fast CH_3 elimination channels operate; (ii) 236 nm, where only the slow channel exists; and (iii) 217 nm where NMP has strong absorption to the dipole-allowed $\pi\pi^*$ state. The excited state molecules were photoionized by a time-delayed femtosecond probe pulse of 267 nm. Dramatic changes in the form of the TRPES spectra were observed for these three different excitation energies, as shown in Fig. 5.

Global 2D least squares fits at all time delays and photoelectron kinetic energies were obtaining using Levenburg-Marquart algorithm.[30] For both 236 nm and 242 nm, a parallel kinetic model with two time constants represents the experimental data very well. Addition of more components only leads to a minor improvement in fit quality. The two time constants are 5.2/87.3 ps for 236 nm, and 5.7/952 ps for 242 nm. Decay associated spectra (DAS) of the two time constants at each wavelength are also derived from the fitting (not shown here). At each wavelength, both DAS have Rydberg-state-like features: a single sharp peak due to $\Delta v = 0$ FC overlap between the neutral Rydberg state and the cationic state; their peaks are also at the same energetic position. All these observations suggest that the two components for each wavelength may come from the same electronic state: the $S_1(^1A_2,\pi\sigma^*)$ state (see Fig. 4). For a pump pulse of 217 nm, a sequential kinetic model with two time constants fits the data very well. The two time constants are $\tau_1 = 101$ fs and $\tau_2 = 353$ fs. The implications of these time constants and fit models are not yet clear. High level theoretical calculations and analysis are currently in progress.[31]

In future experiments, we will measure the kinetic energy distribution of methyl radical to determine the fast *versus* slow branching ratio using the velocity map imaging technique. By studying these as a function of the delay, intensity and polarization of the NRDSE field, we will investigate control over electronic branching at the S_1/S_0 CI. The details of the control experiments will be dependent on the outcomes of current field-free dynamics studies, which continue.

2.4 Quantum coherence amplification

The potential effect of vacuum fluctuations on molecular quantum control was discussed in section 2.2.2. In particular, if spontaneous Raman emission influences a control process then the excited material dynamics will have a fluctuating phase from shot to shot. This poses a general problem in coherent preparation of matter: how to generate large amplitude vibrational or rotational excitations with a predetermined phase such that the dynamics are phase locked to an ultrashort pulse source. Typically, this is achieved *via* impulsive stimulated Raman scattering (ISRS) using a high power ultrashort pulse source, either in the form of a single ultrashort pulse,[10,32,33] or sequence of pulses.[34] In quantum coherence
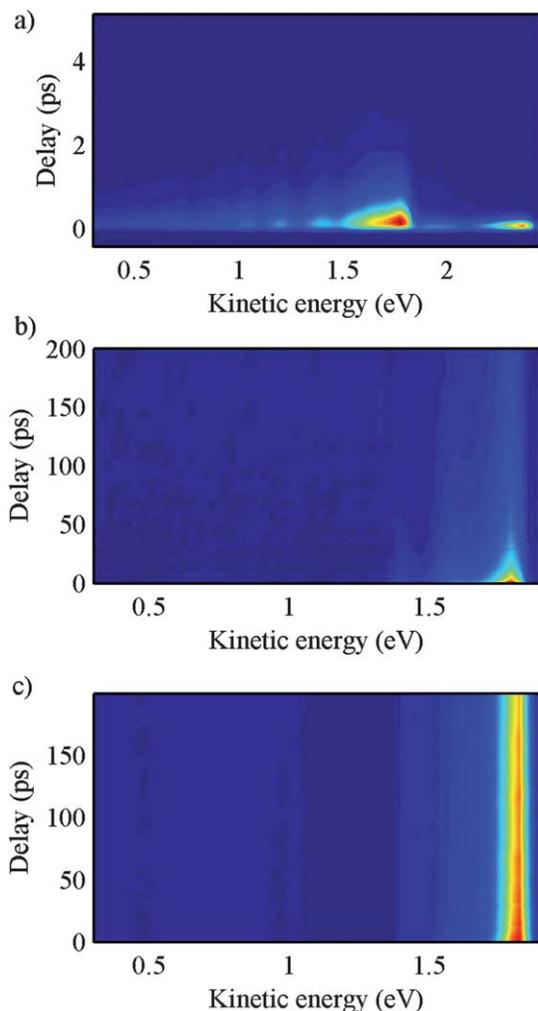
Fig. 5 TRPES spectra of N-methylpyrrole with pump wavelength of a) 217 nm, b) 236 nm, and c) 242 nm are shown (after subtracting background photoelectrons generated from single color multiphoton ionization). The probe wavelength is 267 nm.

amplification,[35] this preparation is achieved in two steps. Initially, a small fraction of energy from the ultrashort pulse is used as a 'seed', to pre-excite the rotational or vibrational levels of the system by ISRS, and dominate the effect of vacuum fluctuations. For ISRS to occur, the ultrashort pulse must have duration shorter than, or comparable to, the ro-vibrational dynamics it is to excite; in the frequency domain this means that the pulse spectrum contains both the pump and Stokes frequencies necessary for Raman scattering. In the next step, a subsequent pump pulse can then amplify the coherence by stimulated Raman scattering. While the pump pulse drives the electrons at optical frequencies, their dynamics are modulated by the pre-existing coherent nuclear motion excited by the seed pulse. As a result, the electronic motion consists of a frequency component at the Stokes frequency, red-shifted from the pump, and Stokes light is emitted. This feedback process continues as the Stokes light stimulates the emission of further Stokes photons, in the process transferring energy from the pump field to the rotational, or vibrational, coherence. Crucially,

because the pre-existing coherence in the medium was generated by the seed, the amplified excitation will be phase-correlated with the ultrashort pulse source rather than with the random vacuum phase. In the absence of the seed, this is not true: spontaneous emission stimulated by the vacuum fluctuations would initiate stimulated Raman scattering and the phase of the excitation would be random on any given laser shot.

A significant advantage of quantum coherence amplification is that the pump pulse source can be completely phase-independent of the ultrashort pulse source, while still preserving phase coherence of the excitation with respect to the latter. While the phase information is provided by the ultrashort pulse source, the majority of the excitation energy is provided by the pump pulse source. In quantum coherence amplification, the pump pulse may be significantly longer than the ultrashort seed pulse, thereby allowing much higher pulse energies to be used while mitigating deleterious nonlinear effects such as field-ionization; such effects can result from coherence preparation using a single high energy, ultrashort excitation pulse.

We have demonstrated quantum coherence amplification on a rotational transition in hydrogen. This implementation may be thought of as an alignment experiment: rather than inducing order along the polarization axis (as in Fig. 3), here the order is induced along the direction of light propagation. In Fig. 6 we show quantum coherence amplification in hydrogen gas, with rotational coherence seeded using a 12 μJ, 55 fs pulse centered at 798 nm, and amplified using a 60 mJ, 10 ns pump pulse at 532 nm. A strong rotational Stokes sideband, shifted from the pump pulse, was detected at the cell output; this indicates that a significant amount of the pump energy had been deposited in the hydrogen molecules as rotational energy. The phase-stability of the rotational coherence with respect to the ultrashort pulse source was tested by scattering a 55 fs probe pulse from the excited molecules. The spectrum of the scattered pulse was measured as a function of delay from an initial starting delay of 3.9 ns. A rotational Stokes sideband, and a rotational anti-Stokes sideband were measured, in addition to the depleted input probe spectrum; energy is transferred from the central probe spectrum into new sidebands by molecular phase modulation.[36,37] Fig. 6 (top) shows a lineout from the centre of the probe spectrum at $\lambda = 798$ nm as a function of delay, while the lower plot shows a corresponding lineout from the rotational sideband at $\lambda = 837$ nm (a shift in wavelength of one rotational quantum). Delay-dependent oscillations are
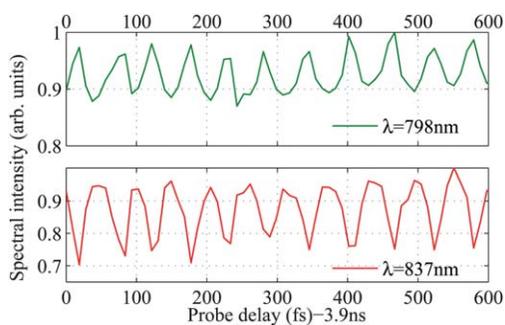

Fig. 6 Plot of delay-dependent oscillations in the spectrum of a probe pulse after phase modulation on propagating through an ensemble of H_2 molecules prepared in a rotationally excited state by quantum coherence amplification. Top: A line-out from the probe spectrum at the central probe wavelength of 798 nm, plotted from an initial delay of 3.9 ns; bottom: the corresponding line-out from the rotational Stokes sideband at 837 nm. The delay-dependent oscillations in the spectral intensity are at the period of the excited rotational transition, and indicate that the coherence is phase-stable with respect to the ultrashort pulse source. Oscillations in the Stokes sideband are π-radians out of phase with those at the central probe wavelength.

apparent in each of the plots, at the period of the excited rotational transition ($\tau_{rot} =$ 57fs). These oscillations demonstrate the phase-stability of the rotational motion with respect to the ultrashort pulse source: when the seed pulse is not present, no oscillations are seen and so the source is not phase-stable. The oscillations in the Stokes sideband are π-radians out of phase with those at the central probe wavelength, with dips in the central probe spectrum resulting from energy transfer into the rotational Stokes sideband.

3. Quantum technologies

In this section, we now move on from the use of the NRDSE in control of chemical systems to discuss its use in the burgeoning domain of quantum technologies. In the two implementations discussed, the main tool for articulating control in the target system is again the laser induced dynamic Stark effect. The application of the effect in these diverse systems indicates its broad utility, not just in quantum control, but also in the development of quantum technologies.

Along with the development of Quantum Theory came the realization that the probabilities associated with quantum systems exhibit features not expected from classical probability theory. Over time it became clear that these violations of classical probability theory actually imply that certain devices may be built with characteristics superior to their classical analogues, including improved algorithm processing and communications protocols. One experimental challenge in building these devices is finding suitable quantum systems and to interact with them in an efficient and precise manner. Various systems have been investigated including propagating photons,[38,39] ions,[40] nuclear spins,[41] high Q-cavities and others.[42] All have appealing features and challenges. To bridge the discussion of quantum control with quantum technologies we briefly conclude by discussing two quantum systems that we have investigated that, when subjected to the off-resonant dynamic Stark effect, can be utilized in the development of quantum technology devices. The first system is a quantum memory in caesium vapour and the second is a room-temperature solid state lambda system in bulk diamond.

3.1. Ensemble quantum memory in caesium

The ability to store quantum information will be a key enabling capability for quantum information processing and communication.[43] In quantum communication, designs for quantum networks require the ability to store and controllably re-emit photons, while preserving their initial quantum characteristics with high fidelity and efficiency. Quantum information processing will utilize 'buffers' to store quantum information deterministically while other information is processed and manipulated, just as in classical computation. Storage of quantum information is more problematic than its classical analogue because the no-cloning theorem prohibits the copying of quantum states. Due to their high speeds and low interaction strengths with the environment, photons are an ideal carrier of quantum information. However, these same features render photons challenging for storage of quantum information: a different physical manifestation of the information is required, such as an atomic or solid-state system. A key challenge is therefore to transfer quantum information from photons to such a system, acting as a storage device or 'quantum memory', with high fidelity.

The storage of quantum light states in an atomic ensemble,[44] for example, requires precise control of the internal atomic dynamics to enable efficient read and write operations on the memory. Here again the dynamic control of energy levels in the storage medium *via* non-resonant fields is a key enabling feature. Recently a high-speed Raman memory protocol has been developed, in which input photons are mapped into a collective atomic exciation by Raman interaction with a much stronger control field.[45] Application of the control field dynamically generates
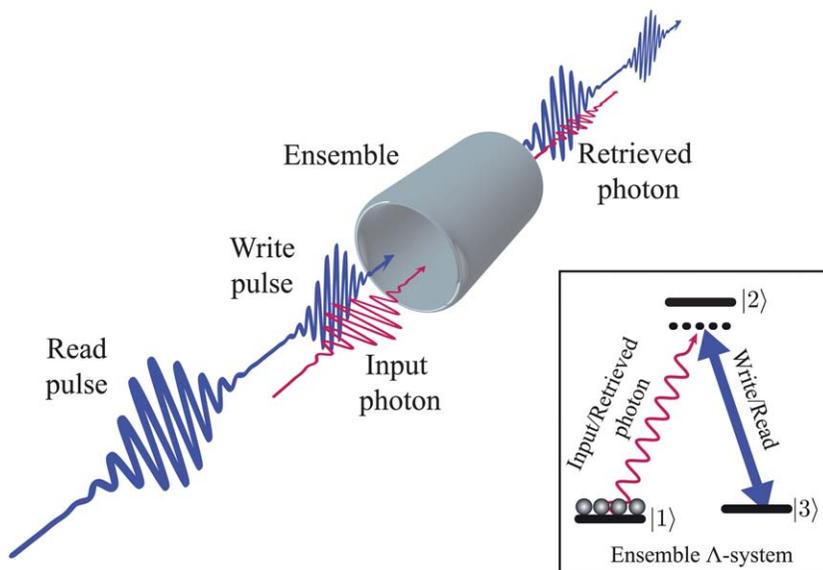
Fig. 7 Ensemble three-level system. The input photon is directed into the ensemble along with a strong write pulse and is stored. A subsequent strong read pulse extracts the stored excitation, mapping it to an output photon. *Inset*: Under appropriate circumstances an ensemble can behave as an individual quantum system, greatly reducing the complexity that would be required to couple to an individual atomic Λ-level structure. In the caesium quantum memory the $F = 3,4$ 'clock states' of the $6^2S_{1/2}$ ground-level hyperfine manifold are the states $|1\rangle$ and $|3\rangle$, and are linked to the excited state $|2\rangle$ ($6^2P_{3/2}$ manifold) through the D2 line at 852 nm. In bulk diamond the ground state $|1\rangle$ is the acoustic phonon and the storage state $|3\rangle$ represents an optical phonon. The transition is then linked *via* the far off resonance exciton state $|2\rangle$.

bandwidth from a narrow transition, enabling the input photons to be absorbed. Subsequent application of a second control field then enables the process to be reversed, and the stored information can be read out.

In the experimental implementation (fig. 7), a 300 ps write pulse and a weak 300 ps input photons pulse are overlapped and directed into a caesium vapour cell. The input photons are mapped *via* a Raman transition into a collective atomic excitation on the hyperfine levels of the caesium vapour. After a delay, a read pulse is sent into the vapour cell and converts the excitation into an optical output signal. Due to the use of an off-resonant Raman interaction which generates bandwidth for storage and read-out of the input photons, the technique has the potential for GHz data rates, a hundred-fold increase over other techniques.

3.2. Ensemble Λ-system in bulk diamond

Due to their intrinsic stability and compactness, efforts continue to develop easily accessed quantum systems with solids. In particular, bulk diamond phonons represent a simple and stable solid-state system in which to investigate quantum phenomena.[46,47] The extraordinary physical and optical properties of diamond make it a model quantum workbench. The workbench can be considered as a room temperature, solid-state, ultra-broadband 'lambda' system where control pulses can be used to write and read photons into and from the optical phonon state. Quantum features are difficult to observe in room temperature solids. Decoherence usually destroys any quantum effects before it can be measured or utilized. However, due to the large splitting between storage states (1332 cm^{-1} between the states $|1\rangle$ and $|3\rangle$), bulk diamond phonons can accommodate femtosecond pulses and therefore demonstrate an unusually high number of operational time bins.

As in the caesium quantum memory, the write process is performed by a control pulse that dynamically generates bandwidth (fig. 7). Unfortunately phonon coherence lifetimes in diamond are 7–11 ps, so the stored phonon rapidly decays. However, although the decay is rapid, the use of femtosecond pulses still permits a significant number of read/write operations (~100) to be performed before coherence is lost. In addition, the loss of system coherence and population in memory can be used to quantify the characteristic decay times T_1 and T_2.[46,47] Performing read and write sequences is a prerequisite to the measurement based entanglement approaches under development. The use of control fields to dynamically generate bandwidth may become a useful tool on the quantum information workbench.

4. Conclusion

Externally applied electric forces provide many strategies for control. The use of the non-resonant dynamic Stark effect (NRDSE), induced by strong near infrared laser fields, is a powerful tool within this class. For example, the NRDSE can be used to align molecules (in both 1D and 3D), in order to make improved (*i.e.* molecular frame) dynamical observations and potentially alter chemical interactions. The NRDSE may also be used to control product branching yields in neutral molecule photodissocation. This is achieved through the application of laser fields that are of sufficient intensity to modify potential energy barriers during the dissociation event. Importantly, this is done without inducing further electronic transitions (*i. e.* the NRDSE is a non-peturbative but non-ionizing—or non-destructive—control strategy). From this point of view, the NRDSE interaction may be viewed as a photonic catalyst rather than a photonic reagent. The extension of NRDSE control of product branching during polyatomic photodissociation is in progress. In many polyatomic systems, multiple conical intersections may be traversed as the initially prepared state evolves towards the final product state distribution and one can perhaps envisage the use of multiple control pulses, each precisely timed, to effect control at several different points along the reaction coordinate.

The links between quantum control and quantum information based technology continue to grow. One example is optical quantum memories which can store and controllably re-emit photons, preserving their initial quantum characteristics with high efficiency and fidelity. These need to be both written and read, and are therefore related to control approaches. For example, the high-speed Raman protocol in caesium uses dynamic Stark shifts to sweep an absorption transition during the storage of a photon, generating bandwidth over an otherwise a narrow transition. This increased bandwidth leads to GHz data rates—a hundred-fold increase over other techniques. Another area is the solid state phonon system in bulk diamond. Again, the dynamically increased bandwidth due to the control pulse interaction provides a novel route to high speed quantum storage, but this time in a compact solid state device that operates at room temperature.

The NRDSE is a general interaction between strong non-resonant light fields and all quantum systems containing charged particles. It is tacitly present in all strong field experiments, but can be utilized as a unique tool in different systems (*e.g.* alignment, product control, quantum memories). We anticipate that further development in control based on NRDSE will continue to open new areas for control and coherence in chemistry, physics and, quantum information science.

References

1 S. Rice and M. Zhao, *Optical control of molecular dynamics*, John Wiley, 2000.
2 M. Shapiro and P. Brumer, *Principles of the quantum control of molecular processes*, Wiley-Interscience, 2003.
3 K. Bergmann, H. Theuer and B. W. Shore, *Rev. Mod. Phys.*, 1998, **70**, 1003–1025.
4 *Conical Intersection: Electronic Structure, Dynamics & Spectroscopy*, ed. W. Domcke, D. R. Yarkony and H. Koppel, World Scientific Publishing Company, 2004.
5 B. J. Sussman, *Am. J. Phys.*, 2011, **79**, 477–484.
6 D. Townsend, B. J. Sussman and A. Stolow, *J. Phys. Chem. A*, 2011, **115**, 357–373.
7 R. Loudon, *The Quantum Theory of Light*, Oxford University press, USA, 2000.
8 H. Stapelfeldt and T. Seideman, *Rev. Mod. Phys.*, 2003, **75**, 543–557.
9 B. Friedrich and D. Herschbach, *Phys. Rev. Lett.*, 1995, **74**, 4623–4626.
10 M. Morgen, W. Price, L. Hunziker, P. Ludowise, M. Blackwell and Y. Chen, *Chem. Phys. Lett.*, 1993, **209**, 1–9.
11 J. P. Heritage, T. K. Gustafson and C. H. Lin, *Phys. Rev. Lett.*, 1975, **34**, 1299–1302.
12 M. G. Raymer and J. Mostowski, *Phys. Rev. A*, 1981, **24**, 1980–1993.
13 M. Raymer and I. A. Walmsley, *Prog. Opt.*, 1990, **28**, 181.
14 D. D. Yavuz, D. R. Walker, G. Y. Yin and S. E. Harris, *Opt. Lett.*, 2002, **27**, 769.
15 Y. Yan, E. Gamble Jr and K. Nelson, *J. Chem. Phys.*, 1985, **83**, 5391–5399.
16 J. G. Underwood, M. Spanner, M. Y. Ivanov, J. Mottershead, B. J. Sussman and A. Stolow, *Phys. Rev. Lett.*, 2003, **90**, 223001.
17 B. J. Sussman, M. Y. Ivanov and A. Stolow, *Phys. Rev. A*, 2005, **71**, 051401.
18 G. Herzberg, *Molecular Spectra and Molecular Structure: 1. Spectra of diatomic molecules*, Van Nostrand, Princeton, 1950.
19 B. J. Sussman, D. Townsend, M. Y. Ivanov and A. Stolow, *Science*, 2006, **314**, 278–281.
20 M. S. Child, *Mol. Phys.*, 1976, **32**, 1495–1510.
21 C. Zhu, Y. Teranishi and H. Nakamura, in *Adv. Chem. Phys.*, ed. I. Prigogine and S. A. Rice, John Wiley & Sons, Inc., 2007, vol. 117, ch. Nonadiabatic transitions due to curve crossings: complete solutions of the Landau–Zener-stueckelberg problems and their applications, pp. 127–233.
22 D. R. Yarkony, *Rev. Mod. Phys.*, 1996, **68**, 985.
23 A. M. D. Lee, J. D. Coe, S. Ullrich, M.-L. Ho, S.-J. Lee, B.-M. Cheng, M. Z. Zgierski, I.-C. Chen, T. J. Martinez and A. Stolow, *J. Phys. Chem. A*, 2007, **111**, 11948–11960.
24 A. G. Sage, M. G. Nix and M. N. R. Ashfold, *Chem. Phys.*, 2008, **347**, 300–308.
25 G. Piani, L. Rubio-Lago, M. A. Collier, T. N. Kitsopoulos and M. Becucci, *J. Phys. Chem. A*, 2009, **113**, 14554–14558.
26 R. McDiarmid and X. Xing, *J. Chem. Phys.*, 1996, **105**, 867–873.
27 A. L. Sobolewski and W. Domcke, *Chem. Phys.*, 2000, **259**, 181–191.
28 M. Vazdar, M. Eckert-Maksic, M. Barbatti and H. Lischka, *Mol. Phys.*, 2009, **107**, 845–854.
29 A. Stolow and J. G. Underwood, in *Adv. Chem. Phys.*, ed. S. A. Rice, John Wiley & Sons, Inc., 2008, vol. 139, ch. Time-Resolved Photoelectron Spectroscopy of Nonadiabatic Dynamics in Polyatomic Molecules, pp. 497–584.
30 K. Levenberg, *Quart. Appl. Math.*, 1944, **2**, 164–168.
31 G. Worth and M. N. R. Ashfold, personal communication.
32 S. D. Silvestri, J. G. Fujimoto, E. P. Ippen, E. B. Gamble, L. R. Williams and K. A. Nelson, *Chem. Phys. Lett.*, 1985, **116**, 146–152.
33 R. Bartels, S. Backus, M. Murnane and H. Kapteyn, *Chem. Phys. Lett.*, 2003, **374**, 326–333.
34 J. P. Cryan, P. H. Bucksbaum and R. N. Coffee, *Phys. Rev. A*, 2009, **80**, 063412.
35 P. J. Bustard, B. J. Sussman and I. A. Walmsley, *Phys. Rev. Lett.*, 2010, **104**, 193902.
36 M. Wittmann, A. Nazarkin and G. Korn, *Phys. Rev. Lett.*, 2000, **84**, 5508.
37 A. V. Sokolov and S. E. Harris, *Journal of Optics B: Quantum and Semiclassical Optics*, 2003, **5**, R1.
38 P. Kok, W. Munro, K. Nemoto, T. Ralph, J. Dowling and G. Milburn, *Rev. Mod. Phys.*, 2007, **79**, 135–174.
39 C. Perez-Delgado and P. Kok, *Arxiv preprint arXiv:0906.4344*, 2009.
40 J. Cirac and P. Zoller, *Phys. Rev. Lett.*, 1995, **74**, 4091–4094.
41 Kane, *Nature*, 1998, **393**, 133–138.
42 H. Mabuchi and A. Doherty, *Science*, 2002, **298**, 1372.
43 A. Lvovsky, B. Sanders and W. Tittel, *Nature Photonics*, 2009, **3**, 706–714.
44 K. Hammerer, A. S. Sørensen and E. S. Polzik, *Rev. Mod. Phys.*, 2010, **82**, 1041–1093.
45 K. Reim, J. Nunn, V. Lorenz, B. Sussman, K. Lee, N. Langford, D. Jaksch and I. Walmsley, *Nature Photonics*, 2010, **4**, 218–221.

46 F. Waldermann, B. Sussman, J. Nunn, V. Lorenz, K. Lee, K. Surmacz, K. Lee, D. Jaksch, I. Walmsley and P. Spizziri, *et al.*, *Phys. Rev. B*, 2008, **78**, 155201.
47 K. Lee, B. J. Sussman, J. Nunn, V. Lorenz, K. Reim, D. Jaksch, I. Walmsley, P. Spizzirri and S. Prawer, *Diamond and Related Materials*, 2010, **19**, 1289–1295.
48 O. Schalk, Private communication (2011).